

Canards in stiction: on solutions of a friction oscillator by regularization*

Elena Bossolini[†], Morten Brøns[†], and Kristian Uldall Kristiansen[†]

Abstract. We study the solutions of a friction oscillator subject to stiction. This discontinuous model is non-Filippov, and the concept of Filippov solution cannot be used. Furthermore some Carathéodory solutions are unphysical. Therefore we introduce the concept of stiction solutions: these are the Carathéodory solutions that are physically relevant, i.e. the ones that follow the stiction law. However, we find that some of the stiction solutions are forward non-unique in subregions of the slip onset. We call these solutions singular, in contrast to the regular stiction solutions that are forward unique. In order to further the understanding of the non-unique dynamics, we introduce a regularization of the model. This gives a singularly perturbed problem that captures the main features of the original discontinuous problem. We identify a repelling slow manifold that separates the forward slipping to forward sticking solutions, leading to a high sensitivity to the initial conditions. On this slow manifold we find canard trajectories, that have the physical interpretation of delaying the slip onset. We show with numerics that the regularized problem has a family of periodic orbits interacting with the canards. We observe that this family has a saddle stability and that it connects, in the rigid body limit, the two regular, slip-stick branches of the discontinuous problem, that were otherwise disconnected.

Key words. Stiction, friction oscillator, non-Filippov, regularization, canard, slip-stick, delayed slip onset

AMS subject classifications. 34A36, 34E15, 34C25, 37N15, 70E18, 70E20

1. Introduction. Friction is a tangential reaction force that appears whenever two rough surfaces are in contact. This energy-dissipating force is desirable in car brakes [5], it occurs at the boundaries of the Earth's crustal plates during fault slip [32, 49], and it causes the sound of string instruments [1, 13]. Friction may initiate undesirable noise, like the squeaking of the chalk on a blackboard, or the squealing of train wheels in tight curves [20]. It may also induce chattering vibrations, as in machine tools [38], and in relay feedback systems [34].

The variety of examples above-mentioned underlines the importance of understanding the friction force, although this is far from being accomplished. For instance, little is known on the shape of the friction law for small velocities, as it is difficult to verify it experimentally [21, 39]. Yet, it is recognized that the maximal value of the friction force at *stick*, that means at zero relative velocity, is higher than at *slip*, when the two surfaces are in relative motion [40]. Several models of friction exist in the literature [35, 36, 48, 49], and most of them are discontinuous at stick, like the stiction model. Stiction defines a maximum *static* friction force during stick and a lower, *dynamic* friction force at slip. In subsets of

*Submitted to the editors March 13, 2017.

Funding:

[†]Department of Applied Mathematics and Computer Science, Technical University of Denmark, Kongens Lyngby 2800, DK (ebos@dtu.dk, mobr@dtu.dk, krkri@dtu.dk).

the discontinuity, the stiction model has solutions that are forward non-unique. In these subsets, a numerical simulation requires a choice of forward integration, possibly discarding solutions.

This manuscript aims to unveil, through a mathematical analysis, new features of the stiction law around the *slip onset*, i.e. when the surfaces start to slip. The manuscript shows that, in certain circumstances, the slip onset is delayed with respect to the instant where the external forces have equalled the maximum static friction. This result, that in principle could be tested experimentally, has physical implications that may further the understanding of phenomena related to friction.

The paper studies the new features of the stiction law in a model of a friction oscillator subject to stiction [41]. This is a discontinuous system, and one may attempt to study it by using the well-developed theory of Filippov [11, 16]. However, it turns out that the model is non-Filippov, and therefore the concept of Filippov solution cannot be used. New concepts of solution of a discontinuous system are introduced, but they lack forward uniqueness in certain subregions of the slip onset. Here it is not possible to predict whether the oscillator will slip or stick in forward time. To deal with the non-uniqueness, a regularization is introduced [25, 42]: this gives a smooth, singularly perturbed problem, that captures the main features of the original problem. Singular perturbation methods [23] can be used to study the regularized system. The lack of uniqueness turns into a high sensitivity to the initial conditions, where a repelling slow manifold separates sticking from slipping solutions. Along this manifold canard-like trajectories appear. These canard trajectories are the ones that delay the slip onset.

It is already known that the friction oscillator may exhibit chaotic [22, 29] and periodic behaviour [8, 34, 37]. The manuscript shows, with a numerical computation, that there exist a family of slip-stick periodic orbits interacting with the canard solutions. This family connects, at the rigid body limit, the two branches of slip-stick orbits of the discontinuous problem. Furthermore the orbits of this family are highly unstable, due to an “explosion” of the Floquet multipliers.

The manuscript is structured as follows. Section 2 presents the model and section 3 studies its geometrical structure. Section 4 introduces a concept of solution that makes sense for the discontinuous model and section 5 introduces the regularization. Section 6 shows slip-stick periodic orbits interacting with the canard solutions. Finally section 7 concludes the manuscript and discusses the results.

2. Model. A friction oscillator consists of a mass M that sits on a rough table, as shown in Figure 1, and that is subject to a periodic forcing $F_\omega(\bar{t}) := -A \sin(\omega \bar{t})$, with A and ω parameters and \bar{t} time. The mass is connected to a spring of stiffness κ , that at rest has zero length. Hence the spring elongation u corresponds to the position of M . Besides, the motion of the mass on the rough table generates a frictional force F that aims to oppose this movement. The system of equations describing the friction oscillator is

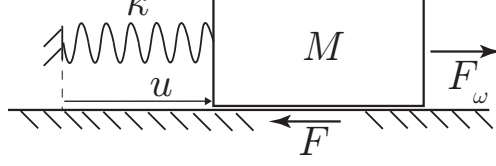


Figure 1: Model of a friction oscillator.

$$(1) \quad \begin{aligned} \dot{u} &= v, \\ M\dot{v} &= -\kappa u + F_\omega(\bar{t}) + F. \end{aligned}$$

The friction force F is modelled as stiction. According to this law, F has different values depending on whether the slip velocity v is zero or not. During slip ($v \neq 0$) stiction is identical to the classical Coulomb law: the friction force is constant and acts in the opposite direction of the relative motion,

$$(2) \quad F = -Nf_d \operatorname{sign} v \quad \text{when} \quad v \neq 0.$$

In equation (2) the parameter N is the normal force, f_d is the dimensionless dynamic friction coefficient, and the sign function is defined as

$$\operatorname{sign} \alpha := \begin{cases} 1 & \text{if } \alpha > 0, \\ -1 & \text{if } \alpha < 0. \end{cases}$$

Figure 2(a) illustrates the slipping law (2). For zero slip velocity ($v = 0$), it is necessary to consider whether this happens on a whole time interval or only instantaneously, i.e. whether \dot{v} is also zero or not. The former case ($v = \dot{v} = 0$) defines the stick phase, and from (1) it follows that

$$(3) \quad F = w(\bar{t}, u) \quad \text{when} \quad v = 0 \quad \text{and} \quad |w| < Nf_s,$$

where $w(\bar{t}, u) := \kappa u - F_\omega(\bar{t})$ is the sum of forces that induce the motion of M . The parameter f_s in (3) is the dimensionless static friction coefficient and $f_s > f_d > 0$ [40]. The idea is that the value of the static friction is exactly the one that counteracts the other forces acting on M , so that the mass will keep on sticking. However the static friction (3) can only oppose the motion of M up to the maximum static friction $\pm Nf_s$, thus

$$F = Nf_s \operatorname{sign} w \quad \text{when} \quad v = 0 \quad \text{and} \quad |w| > Nf_s.$$

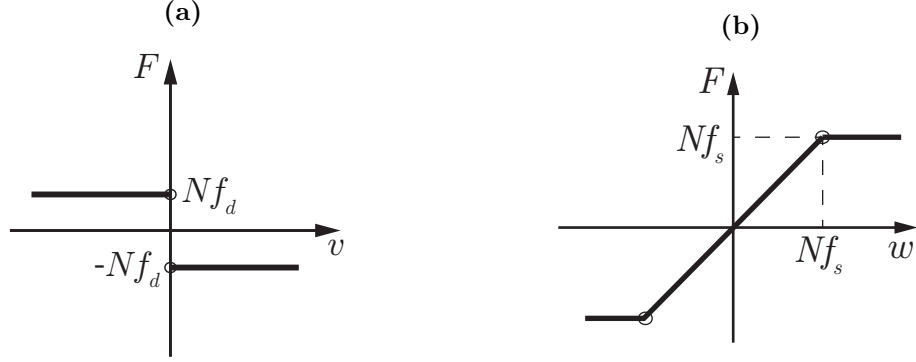


Figure 2: Stiction friction $F(v, w)$. (a): $v \neq 0$. (b): $v = 0$.

In this latter case the friction force is not sufficient to maintain $\dot{v} = 0$ and therefore the mass will slip in forward time. Figure 2(b) illustrates the friction law for $v = 0$. In compact form, stiction is written as:

$$F(v, w) = \begin{cases} -Nf_d \operatorname{sign} v & v \neq 0, \\ w & v = 0 \text{ and } |w| < Nf_s, \\ Nf_s \operatorname{sign} w & v = 0 \text{ and } |w| > Nf_s. \end{cases}$$

The friction law is not defined for $v = 0$ and $|w| = Nf_s$, where the external forces equal the maximum static friction during stick. Other modelling choices may fix a value of F in these points. These choices do not affect the results of the following analysis, see section 4. By rescaling

$$u = \frac{V}{\omega}x, \quad v = Vy, \quad \bar{t} = \frac{t}{\omega},$$

system (1) is rewritten in its dimensionless form:

$$(4) \quad \begin{aligned} x' &= y, \\ y' &= -\xi(x, \theta) + \mu(y, \xi(x, \theta)), \\ \theta' &= 1, \end{aligned}$$

where $\theta \in \mathbb{T}^1$ is a new variable describing the phase of the periodic forcing, and that makes system (4) autonomous. Furthermore

$$\xi(x, \theta) := \frac{w}{A} = \gamma^2 x + \sin \theta,$$

is the sum of the rescaled external forces, and it is often referred to as ξ in the following analysis. In this new system the prime has the meaning of differentiation with respect

to the time t , and $\gamma := \Omega/\omega$ is the ratio between the natural frequency of the spring $\Omega := \sqrt{\kappa/M}$ and the forcing frequency ω . Therefore $\gamma \rightarrow \infty$ corresponds to the rigid body limit. The function μ describes the dimensionless stiction law:

$$(5) \quad \mu(y, \xi) = \begin{cases} -\mu_d \operatorname{sign} y & y \neq 0, \\ \xi & y = 0 \text{ and } |\xi| < \mu_s, \\ \mu_s \operatorname{sign} \xi & y = 0 \text{ and } |\xi| > \mu_s, \end{cases}$$

where $\mu_{d,s} := Nf_{d,s}/A$. System (4) together with the friction function (5) is the model used in the rest of the analysis. In compact form it is written as $z' = Z(z)$, where $z := (x, y, \theta) \in \mathbb{R}^2 \times \mathbb{T}^1$, and $\mathbb{T}^1 := \mathbb{R}/2\pi\mathbb{Z}$. The vector field $Z(z)$ is not defined on the two lines $\{y = 0, \xi = \pm\mu_s\}$. Section 3 studies the phase space of (4) using geometrical tools from piecewise-smooth theory [11, 16].

3. Geometric analysis of the discontinuous system. This section analyses the friction oscillator (4) with stiction friction (5) in the context of piecewise-smooth dynamical systems. The notation is consistent with the one in [18]. System (4) is smooth in the two regions

$$G^+ := \{(x, y, \theta) \in \mathbb{R}^2 \times \mathbb{T}^1 \mid y > 0\}, \\ G^- := \{(x, y, \theta) \in \mathbb{R}^2 \times \mathbb{T}^1 \mid y < 0\}.$$

Let $Z^+(z)$ ($Z^-(z)$) be the vector field $Z(z)$ restricted to G^+ (G^-) and extended to the closure of G^+ (G^-). These two smooth vector fields have the explicit form

$$Z^\pm = \begin{cases} x' & = y, \\ y' & = -\xi(x, \theta) \mp \mu_d, \\ \theta' & = 1. \end{cases}$$

The set $\Sigma := \{(x, y, \theta) \in \mathbb{R}^2 \times \mathbb{T}^1 \mid y = 0\}$ is a surface of discontinuity of $Z(z)$ and it is called the *switching manifold*. The vector field $Z(z)$ is well-defined in $\Sigma \setminus \{\xi = \pm\mu_s\}$ and its dynamics on the y -coordinate is

$$y' = -\xi(x, \theta) + \mu(0, \xi(x, \theta)) \begin{cases} > 0 & \text{for } \xi < -\mu_s, \\ = 0 & \text{for } |\xi| < \mu_s, \\ < 0 & \text{for } \xi > \mu_s. \end{cases}$$

Therefore it is natural to subdivide Σ into the three sets

$$\Sigma_c^+ := \{(x, y, \theta) \in \mathbb{R}^2 \times \mathbb{T}^1 \mid y = 0 \text{ and } \xi < -\mu_s\}, \\ \Sigma_s := \{(x, y, \theta) \in \mathbb{R}^2 \times \mathbb{T}^1 \mid y = 0 \text{ and } -\mu_s < \xi < \mu_s\}, \\ \Sigma_c^- := \{(x, y, \theta) \in \mathbb{R}^2 \times \mathbb{T}^1 \mid y = 0 \text{ and } \xi > \mu_s\},$$

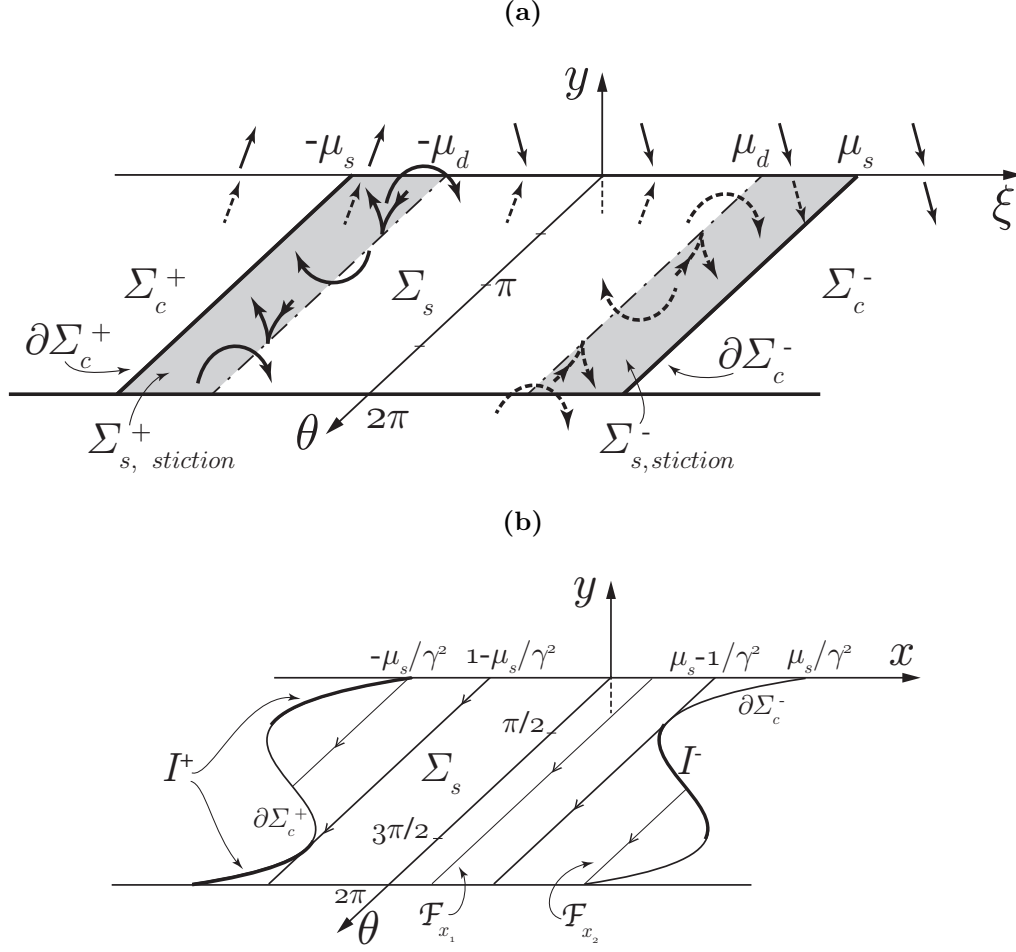


Figure 3: (a): Vector fields Z^\pm and their tangencies at $\xi = \mp\mu_d$ in the (ξ, y, θ) -space. Z^- is dashed because it is below Σ_s . The grey bands indicate where Z^\pm suggest crossing but instead the solution for $y = 0$ is sticking. (b): Phase space of Z_s in the (x, y, θ) -space with the tangencies at $\theta = \{\pi/2, 3\pi/2\}$. The leaf \mathcal{F}_{x_1} is a full circle, while \mathcal{F}_{x_2} is an arc of a circle. The intervals of non-uniqueness I^\pm are introduced in Proposition 4.4.

that are shown in Figure 3(a). The set Σ_c^+ (Σ_c^-) is called the *crossing region pointing upwards (downwards)*, because orbits here switch from G^- to G^+ (from G^+ to G^-). The strip Σ_s is called the *sticking region* because trajectories within it are not allowed to switch to G^\pm , and they correspond to solutions where the mass sticks to the table. Let $Z_s(z)$ be the smooth vector field $Z(z)$ restricted to Σ_s and extended to the closure of Σ_s . This two-dimensional vector field has the explicit form $(x, \theta)' = (0, 1)$, thus Σ_s is foliated by

invariant arcs of circles

$$(6) \quad \mathcal{F}_{x_0} := \{(x, y, \theta) \in \Sigma_s \mid x = x_0\},$$

since $\theta \in \mathbb{T}^1$. [Figure 3\(b\)](#) shows the foliation \mathcal{F}_{x_0} . The boundaries of Σ_s with Σ_c^\pm define the two sets

$$\begin{aligned} \partial\Sigma_c^+ &:= \{(x, y, \theta) \in \mathbb{R}^2 \times \mathbb{T}^1 \mid y = 0 \text{ and } \xi = -\mu_s\}, \\ \partial\Sigma_c^- &:= \{(x, y, \theta) \in \mathbb{R}^2 \times \mathbb{T}^1 \mid y = 0 \text{ and } \xi = \mu_s\}. \end{aligned}$$

The vector field $Z(z)$ is not defined on $\partial\Sigma_c^\pm$, but the three vector fields $Z_s(z)$ and $Z^\pm(z)$ are. Indeed $\partial\Sigma_c^\pm$ belong to the closure of both Σ_s and G^\pm . Hence on $\partial\Sigma_c^\pm$ solutions may be forward non-unique. This will be discussed in [section 4](#).

The following two [Propositions 3.2](#) and [3.4](#) say where the vector fields $Z_s(z)$, $Z^\pm(z)$ are tangent to $\partial\Sigma_c^\pm$ and Σ respectively. The results are shown in [Figure 3](#). First, a definition introduces the concepts of visible and invisible tangency.

Definition 3.1. Let $\hat{\Sigma} := \{z \in \mathbb{R}^n \mid \chi(z) > 0\}$, where $\chi : \mathbb{R}^n \rightarrow \mathbb{R}$ is a smooth and regular function such that $\nabla\chi(z) \neq 0$ for every $z \in \mathbb{R}^n$. Furthermore let $\hat{Z} : \hat{\Sigma} \rightarrow \mathbb{R}^n$ be a smooth vector field, having a smooth extension to the boundary of $\hat{\Sigma}$, that is for $\chi(z) = 0$. In addition, let $\mathcal{L}_{\hat{Z}}\chi(z) := \nabla\chi \cdot \hat{Z}(z)$ denote the Lie derivative of χ with respect to $\hat{Z}(z)$. The vector field $\hat{Z}(z)$ is tangent to the set $\chi(z) = 0$ at $p \in \hat{\Sigma}$ if $\mathcal{L}_{\hat{Z}}\chi(p) = 0$. The tangency is called visible (invisible) if $\mathcal{L}_{\hat{Z}}^2\chi(p) > 0$ ($\mathcal{L}_{\hat{Z}}^2\chi(p) < 0$), where $\mathcal{L}_{\hat{Z}}^2\chi(p)$ is the second order Lie derivative. The tangency is a cusp if $\mathcal{L}_{\hat{Z}}^2\chi(p) = 0$ but $\mathcal{L}_{\hat{Z}}^3\chi(p) \neq 0$.

In other words, the tangency is visible if the orbit $z' = \hat{Z}(z)$ starting at p stays in $\hat{\Sigma}$ for all sufficiently small $|t| > 0$, and it is invisible if it never does so [[11](#), p. 93 and p. 237]. A quadratic tangency is also called a *fold* [[45](#)].

Proposition 3.2. $Z_s(z)$ is tangent to $\partial\Sigma_c^-$ ($\partial\Sigma_c^+$) in the isolated points $\theta \in \{\pi/2, 3\pi/2\}$. The tangency is visible (invisible) for $\theta = \pi/2$, and invisible (visible) for $\theta = 3\pi/2$.

Proof. Define the function $\chi(\xi, \theta) = \mu_s - \xi(x, \theta)$ so that it is defined within Σ , and its zeroes belong to $\partial\Sigma_c^-$. Then $\mathcal{L}_{Z_s}\chi(p) = 0$ in $\theta = \{\pi/2, 3\pi/2\}$. Moreover $\mathcal{L}_{Z_s}^2\chi(p) = \sin\theta$. Hence $\theta = \pi/2$ ($\theta = 3\pi/2$) is a visible (invisible) fold. Similar computations prove the result for $\partial\Sigma_c^+$. ■

Corollary 3.3. If $\mu_s > 1$, then the invariant leaves \mathcal{F}_x of [\(6\)](#) with $|\gamma^2x| < \mu_s - 1$ are periodic with period 2π . The remaining leaves of [\(6\)](#), having $|\gamma^2x| \geq \mu_s - 1$, escape Σ_s in finite time. If $\mu_s < 1$ no periodic solutions exist on Σ_s .

Proof. The sticking trajectory $\gamma^2x(t) = \mu_s - 1$ ($\gamma^2x(t) = -\mu_s + 1$) is tangent to $\partial\Sigma_c^-$ ($\partial\Sigma_c^+$) because $\xi(x, \pi/2) = \mu_s$ ($\xi(x, 3\pi/2) = -\mu_s$). These two lines coincide for $\mu_s = 1$. When $\mu_s > 1$ the orbits $|\gamma^2x(t)| < \mu_s - 1$ are included within the two tangent orbits. Hence they never intersect the boundaries $\partial\Sigma_c^\pm$ and therefore are periodic with period 2π . Instead, the trajectories $\mu_s > |\gamma^2x(t)| \geq \mu_s - 1$ exit Σ_s in finite time. ■

The orbit $\mathcal{F}_{x_1} \subset \Sigma_s$ of Figure 3(b) is periodic, while \mathcal{F}_{x_2} leaves Σ_s in finite time. The period $T = 2\pi$ corresponds to a period $\bar{T} = 2\pi/\omega$ in the original time \bar{t} , as it is often mentioned in the literature [8, 41]. The condition $\mu_s > 1$ corresponds to $Nf_s > A$ that is, the maximum static friction force is larger than the amplitude of the forcing F_ω . This interpretation makes it an obvious condition for having sticking solutions.

Proposition 3.4. *The vector field Z^- (Z^+) is tangent to Σ on the line $\xi = \mu_d$ ($\xi = -\mu_d$). The tangency is invisible (visible) for $\theta \in]\pi/2, 3\pi/2[$, it is visible (invisible) for $\theta \in [0, \pi/2[$ and $\theta \in]3\pi/2, 2\pi[$, while it is a cusp on the isolated points $\theta = \{\pi/2, 3\pi/2\}$.*

Proof. Define the function $\chi(x, y, \theta) = -y$ so that it is defined in G^- and it is zero in Σ . Then $\mathcal{L}_{Z^-}\chi(p) = \xi(x, \theta) - \mu_d = 0$ on the line $\xi = \mu_d$, $\theta \in \mathbb{T}^1$. Moreover $\mathcal{L}_{Z^-}^2\chi(p) = \cos\theta$. This is negative for $\theta \in]\pi/2, 3\pi/2[$ and positive for $\theta \in [0, \pi/2[$ and $\theta \in]3\pi/2, 2\pi[$. The points $\theta = \pi/2$ and $\theta = 3\pi/2$ have $\mathcal{L}_{Z^-}^2\chi(p) = 0$ but $\mathcal{L}_{Z^-}^3\chi(p) \neq 0$. Similar computations prove the result for $Z^+(z)$. ■

The knowledge of the tangencies is sufficient to describe the local phase space of system (4) around the discontinuity Σ , as Figure 3 shows. Section 4 discusses how forward solutions of $Z(z)$, that are smooth within each set G^\pm and Σ_s , connect at the boundaries of these regions. It is futile to study solutions in backwards time, because when an orbit lands on Σ_s , the information of when it has landed is lost.

4. Forward solutions of the discontinuous system. Classical results on existence and uniqueness of solutions require Lipschitz continuous right hand sides, and therefore do not apply to discontinuous systems like (4). A class of discontinuous systems for which some results are known, is the one of Filippov-type [16]. In a Filippov-type system the vector fields $Z^\pm(z)$ are sufficient to describe the dynamics within the switching manifold Σ . This is useful especially when there is no vector field already defined on Σ . Let $Z_y^\pm(z)$ be the y component of $Z^\pm(z)$ in a point $z \in \Sigma$. Then Filippov's convex method defines the *crossing region* as the subset of Σ where $Z_y^+ \cdot Z_y^-(z) > 0$, while the *sliding region* $\Sigma_{s,\text{Filippov}}$ satisfies $Z_y^+ \cdot Z_y^-(z) < 0$ [16, § 2], [11, p. 76]. The idea is that solutions inside the sliding region cannot exit Σ because $Z^\pm(z)$ do not allow it.

Remark 4.1. System (4) together with the friction law (5) is not of Filippov-type. Indeed the sliding region of system (4) is

$$\Sigma_{s,\text{Filippov}} := \{(x, y, \theta) \in \mathbb{R}^2 \times \mathbb{T}^1 \mid y = 0 \text{ and } -\mu_d < \xi < \mu_d\},$$

that is a strip within Σ_s whenever $\mu_d < \mu_s$. In the two remaining bands

$$\begin{aligned} \Sigma_{s,\text{stiction}}^- &:= \{(x, y, \theta) \in \mathbb{R}^2 \times \mathbb{T}^1 \mid y = 0 \text{ and } \xi \in]\mu_d, \mu_s[\}, \\ \Sigma_{s,\text{stiction}}^+ &:= \{(x, y, \theta) \in \mathbb{R}^2 \times \mathbb{T}^1 \mid y = 0 \text{ and } \xi \in]-\mu_s, -\mu_d[\}, \end{aligned}$$

that are coloured in grey in Figure 3(a), the vector field $Z_s(z)$ does not belong to the convex closure of $Z^\pm(z)$. Here Filippov's method predicts orbits to switch from G^+ to G^- or vice

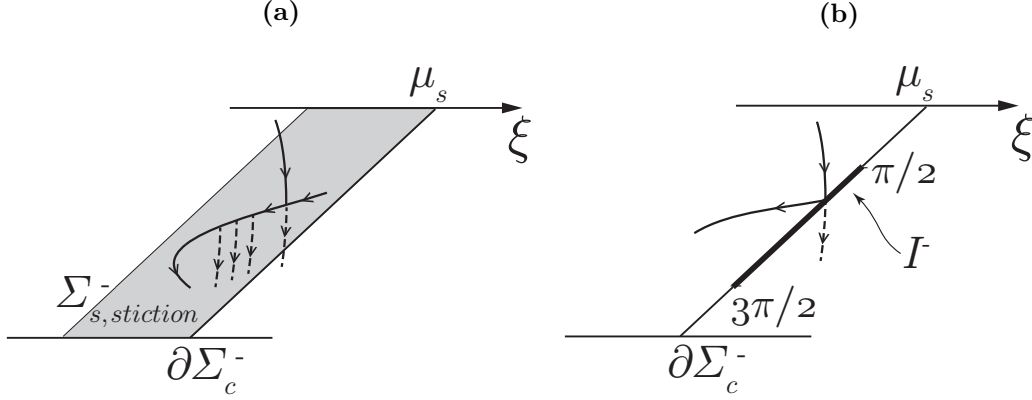


Figure 4: (a): A Carathéodory solution with a pathological non-determinacy of the forward motion on the grey band. (b): Stiction solutions interacting with the line of forward non-uniqueness I^- .

versa, but the actual solution of model (4) lies within Σ_s . When $\mu_d = \mu_s$ the friction law (5) equals the classical Coulomb friction and Σ_s coincides with $\Sigma_{s, \text{Filippov}}$. This case has been studied in [9, 18, 24].

The two grey bands $\Sigma_{s, \text{stiction}}^\pm$ are unstable to perturbations in y . Consider for instance a trajectory in $\Sigma_{s, \text{stiction}}^-$ that is pushed to G^- by an arbitrary small perturbation: this solution will evolve far from $\Sigma_{s, \text{stiction}}^-$ by following $Z^-(z)$.

Another notion of forward solution of a discontinuous system is the *Carathéodory solution* [7], [16, §1]. This is an absolutely continuous function $z(t)$ that satisfies

$$(7) \quad z(t) = z(0) + \int_0^t Z(z(s)) ds, \quad t \geq 0,$$

where the integral is in a Lesbegue sense. Hence in order to have a Carathéodory solution, $Z(z)$ needs only to be defined almost everywhere.

Proposition 4.2. *For every $z_0 = z(0) \in \mathbb{R}^2 \times \mathbb{T}^1$ there exists a global forward Carathéodory solution of model (4) satisfying (7) for every $t \geq 0$.*

Proof. For every z_0 there exists at least one local classical solution of either $Z^\pm(z)$ or $Z_s(z)$. A forward solution of (7) is obtained by piecing together such local orbits together on Σ . This can be done for every $t > 0$ since $Z^\pm(z)$ and $Z_s(z)$ are each linear in (x, y) , excluding the possibility of blowup in finite time. ■

Not every forward Carathéodory solution has a physical meaning. Consider for instance a trajectory that under the forward flow (4) lands inside $\Sigma_{s, \text{stiction}}^-$, as shown in Figure 4(a). There are two ways to obtain a forward solution at this point: either leave Σ and follow the

vector field $Z^-(z)$, or remain on Σ_s . Besides, the forward trajectory on Σ_s may switch to G^- at any point within $\Sigma_{s,\text{stiction}}^-$. The orbits switching to G^- appear to be mathematical artifacts, as they do not satisfy the condition $|\xi| > \mu_s$ of the stiction law (5). There is a need to have a concept of solution that discards all these pathologies. The following definition does so, by using a “minimal” approach.

Definition 4.3. A stiction solution $t \mapsto z(t)$, with $t \geq 0$, is a Carathéodory solution that leaves Σ_s only at the boundaries $\partial\Sigma_c^\pm$.

A stiction solution is called singular if for some $t_1 \geq 0$ the point $z(t_1)$ belongs to one of the following sets

$$\begin{aligned} I^+ &:= \{(x, y, \theta) \in \mathbb{R}^2 \times \mathbb{T}^1 \mid \xi = -\mu_s, y = 0, \theta \in [\pi/2, 3\pi/2] \}, \\ I^- &:= \{(x, y, \theta) \in \mathbb{R}^2 \times \mathbb{T}^1 \mid \xi = \mu_s, y = 0, \theta \in [0, \pi/2] \cup [3\pi/2, 2\pi[\}. \end{aligned}$$

Otherwise, the stiction solution is called regular.

The sets I^\pm belong to the boundary lines $\partial\Sigma_c^\pm$. Three vector fields are defined on $\partial\Sigma_c^\pm$: $Z_s(z)$ and $Z^\pm(z)$. In particular on both I^\pm the vector field $Z_s(z)$ points inside Σ_s , as it follows from Proposition 3.2, compare with Figure 3(b). Proposition 4.4 describes the existence and uniqueness of stiction solutions for model (4).

Proposition 4.4. There exists a stiction solution $z(t)$ of problem (4) for any initial condition $z_0 = z(0) \in \mathbb{R}^2 \times \mathbb{T}^1$. Regular stiction solutions are forward unique, while singular stiction solutions are forward non-unique.

Proof. Stiction solutions are Carathéodory solutions, hence they exist. Consider a trajectory $z(t)$ that reaches I^- at a time t_1 , as shown in Figure 4(b). Two different forward solutions satisfy (7): either leave Σ and follow the vector field $Z^-(z)$, or remain on Σ_s . Hence the singular stiction solution is forward non-unique. Similarly for I^+ . On the contrary, if $z(t) \notin I^\pm$ at any $t \geq 0$, then there is always only one way to piece together the vector fields at the boundaries $\partial\Sigma_c^\pm$ and therefore $z(t)$ is forward unique. ■

The non-uniqueness of models with stiction friction has been mentioned in [4, 35], without any further explanation. It is not possible to predict whether, for singular stiction solutions, the mass will slip or stick in forward time. Hence numerical simulations that use stiction friction have to make a choice at the points of non-uniqueness to compute the forward flow, often without noticing that a choice is made. This means that solutions may unawarely be discarded. Section 5 investigates the non-uniqueness by regularization.

5. Regularization. A regularization of the vector field $Z(z)$ is a 1-parameter family $Z_\varepsilon(z)$ of smooth vector fields defined by

$$(8) \quad Z_\varepsilon(z) := \frac{1}{2}Z^+(z)(1 + \phi(\varepsilon^{-1}y)) + \frac{1}{2}Z^-(z)(1 - \phi(\varepsilon^{-1}y)),$$

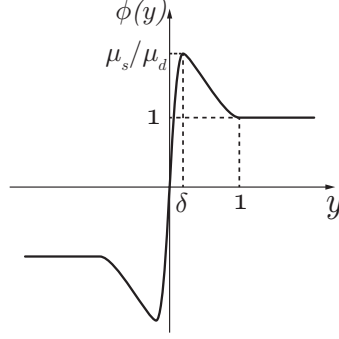


Figure 5: A regularization function $\phi(y)$.

for $0 < \varepsilon \ll 1$. The function $\phi(y)$ is an odd, C^k -function ($1 \leq k \leq \infty$) that satisfies

$$(9) \quad \phi(y) = \begin{cases} 1, & y \geq 1, \\ \mu_s/\mu_d, & y = \delta, \end{cases} \quad \text{and} \quad \phi'(y) \begin{cases} > 0, & 0 < y < \delta, \\ = 0, & y = \delta, \\ < 0, & \delta < y < 1, \end{cases} \quad \phi''(\delta) < 0,$$

where $0 < \delta < 1$. This function is shown in [Figure 5](#). The regularized problem $z' = Z_\varepsilon(z)$ has the advantages of being smooth, and of approximating the discontinuous problem (4) for $0 < \varepsilon \ll 1$. In particular, by the first property of (9), it follows that $Z_\varepsilon(z) = Z^\pm(z)$ for $y \gtrless \pm\varepsilon$, so that the two problems coincide outside of the *region of regularization* $y \in]-\varepsilon, \varepsilon[$. In non-compact form $z' = Z_\varepsilon(z)$ is the singularly perturbed problem

$$(10) \quad \begin{aligned} x' &= y, \\ y' &= -\xi(x, \theta) - \mu_d \phi(\varepsilon^{-1}y), \\ \theta' &= 1, \end{aligned}$$

with $\xi(x, \theta) = \gamma^2 x + \sin \theta$ the function introduced in [section 2](#). When solutions of (10) enter the region of regularization, it is easier to follow them in the rescaled coordinate $\hat{y} = \varepsilon^{-1}y$ so that $y = \pm\varepsilon$ become $\hat{y} = \pm 1$. In the new scale, system (10) becomes the multiple time scales problem

$$(11) \quad \begin{aligned} x' &= \varepsilon \hat{y}, \\ \varepsilon \hat{y}' &= -\xi(x, \theta) - \mu_d \phi(\hat{y}), \\ \theta' &= 1, \end{aligned}$$

that is also known as the *slow problem* [23, 28]. By introducing the fast time $\tau := t/\varepsilon$, system (11) is equivalent to the *fast problem*

$$(12) \quad \begin{aligned} \dot{x} &= \varepsilon^2 \hat{y}, \\ \dot{\hat{y}} &= -\xi(x, \theta) - \mu_d \phi(\hat{y}), \\ \dot{\theta} &= \varepsilon, \end{aligned}$$

with the overdot meaning the differentiation with respect to the fast time τ . The parameter ε measures both the perturbation from the discontinuous system, as in equation (8), and the separation of the time scales. The standard procedure for solving multiple time scales problems is to combine the solutions of the *layer problem*

$$(13) \quad \dot{\hat{y}} = -\xi(x, \theta) - \mu_d \phi(\hat{y}), \quad (x, \theta)(\tau_0) = (x_0, \theta_0),$$

with the ones of the *reduced problem*

$$(14) \quad \begin{aligned} x' &= 0, \\ 0 &= -\xi(x, \theta) - \mu_d \phi(\hat{y}), \\ \theta' &= 1, \end{aligned}$$

where (13) and (14) are the limit for $\varepsilon \rightarrow 0$ of the fast and slow problems (12) and (11). The set of fixed points of the layer problem (13) is called the *critical manifold*

$$(15) \quad C_0 := \{(x, \hat{y}, \theta) \in \mathbb{R}^2 \times \mathbb{T}^1 \mid \xi(x, \theta) + \mu_d \phi(\hat{y}) = 0\},$$

and the solutions of the reduced problem (14) are constrained to it. The critical manifold is said to be *normally hyperbolic* in the points where

$$\left. \frac{\partial \dot{\hat{y}}}{\partial \hat{y}} \right|_{C_0} = -\mu_d \phi'(\hat{y}^{C_0})$$

is non zero, and $\hat{y}^{C_0} = \phi^{-1}(-\xi(x, \theta)/\mu_d)$. It follows that C_0 is not normally hyperbolic on the two *fold lines*

$$f^\pm := \{(x, \hat{y}, \theta) \in \mathbb{R}^2 \times \mathbb{T}^1 \mid \xi = \mp \mu_s, \hat{y} = \pm \delta\}.$$

These lines separate C_0 into the three invariant sets of (13)

$$\begin{aligned} C_r^+ &:= \{(x, \hat{y}, \theta) \in C_0 \mid \delta < \hat{y} < 1\}, \\ C_a &:= \{(x, \hat{y}, \theta) \in C_0 \mid -\delta < \hat{y} < \delta\}, \\ C_r^- &:= \{(x, \hat{y}, \theta) \in C_0 \mid -1 < \hat{y} < -\delta\}, \end{aligned}$$

as shown in Figure 6, where C_a is attracting and C_r^\pm are repelling. Notice that C_a is a graph $\hat{y} \in]-\delta, \delta[$ over Σ_s , while C_r^+ (C_r^-) is a graph $\hat{y} \in]\delta, 1[$ ($\hat{y} \in]-1, -\delta[$) over $\Sigma_{s, \text{stiction}}^+$ ($\Sigma_{s, \text{stiction}}^-$). In terms of (x, y, θ) , these sets collapse onto Σ_s and $\Sigma_{s, \text{stiction}}^\pm$ respectively as $\varepsilon \rightarrow 0$, since $y = \varepsilon \hat{y}$. Similarly, f^\pm collapse onto $\partial \Sigma_c^\pm$. This means that in the (x, y, θ) -space it is not possible to distinguish whether a trajectory belongs to C_a or to C_r^\pm for $\varepsilon = 0$.

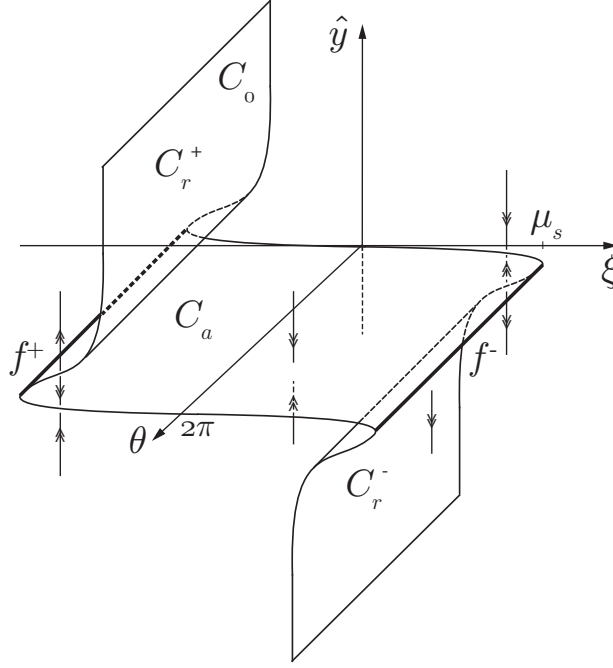


Figure 6: Critical manifold C_0 and its stability properties. In bold: f^\pm . The double arrow denotes dynamics in the fast time τ .

Proposition 5.1. *The reduced problem on C_0 coincides with the vector field $Z_s(z)$ on Σ_s .*

The proof is straightforward since the reduced problem, once constrained to C_0 , is $(x', \theta') = (0, 1)$. From this Proposition, and the fact that $Z_\varepsilon(z) = Z^\pm(z)$ for $y \gtrless \pm\varepsilon$, it follows that the regularized problem (10) captures all the main features of the discontinuous vector field (4) for $\varepsilon \rightarrow 0$. Furthermore, when $0 < \varepsilon \ll 1$ the solutions of (10) are uniquely defined, so that the issue of non-uniqueness of (4) is eliminated. Proposition 5.1 also motivates the conditions (9) for the function $\phi(y)$, as explained in the following Remark.

Remark 5.2. The well known Sotomayor and Teixeira (ST) regularization, considers a regularization function $\phi^{ST}(y)$ that is monotonously increasing in $y \in]-1, 1[$ [42]. At the singular limit, the regularization $Z_\varepsilon^{ST}(z)$ has an attracting invariant manifold C_a^{ST} that is a graph of \hat{y} over $\Sigma_{s, \text{Filippov}}$ [25, 30]. In terms of (x, y, θ) this set collapses onto $\Sigma_{s, \text{Filippov}}$ instead of Σ_s , and hence $Z_\varepsilon^{ST}(z)$ does not tend to $Z(z)$ as $\varepsilon \rightarrow 0$. For this reason the ST regularization is inadequate for model (4).

The results of Fenichel [14, 15] guarantee that for $\varepsilon = 0$, a normally hyperbolic, compact and invariant manifold $S_0 \subset C_0$ perturbs into a non-unique and invariant *slow manifold* S_ε , that is ε -close to S_0 for ε sufficiently small. Furthermore, system (12) has an invariant foliation with base on S_ε , that is a perturbation of the foliation of the layer problem (13)

with base on S_0 .

Let $\varphi_t(z_0)$ be a regular stiction solution of model (4) with initial condition in z_0 , and let $\varphi_t^\varepsilon(z_0)$ be the solution of the regularized problem (10) for the same initial condition. The following statement relates these two solutions.

Proposition 5.3. *For any $T > 0$ there exists an $\varepsilon_0 > 0$ such that the distance between the two solutions $\varphi_t^\varepsilon(z_0)$ and $\varphi_t(z_0)$ is bounded by: $|\varphi_t^\varepsilon(z_0) - \varphi_t(z_0)| \leq c(T)\varepsilon^{2/3}$ for $t \in [0, T]$, where $c(T)$ is a constant that depends upon T , and $0 < \varepsilon \leq \varepsilon_0$.*

Proof. Fenichel's theorems guarantee that, sufficiently far from the fold lines f^\pm , the orbit $\varphi_t^\varepsilon(z_0)$ of the slow-fast problem (11) is $\mathcal{O}(\varepsilon)$ -close to the singular trajectory $\varphi_t(z_0)$. At the folds f^\pm , if at the singular level the solutions are unique, the result by Szmolyan and Wechselberger [44, Theorem 1] guarantees that the distance between the two trajectories is bounded by $\mathcal{O}(\varepsilon^{2/3})$ for a finite time interval T . This is the case of regular stiction solutions. ■

The following Proposition relates the family of sticking solutions of Corollary 3.3 with a family of trajectories on the slow manifold for the regularized problem. For this, define $S_a \subset C_a$ as the compact, invariant, normally hyperbolic set $S_a := \{(x, \hat{y}, \theta) \in \mathbb{R}^2 \times \mathbb{T}^1 \mid |\gamma^2 x| \leq \mu_s - 1 - c, \xi(x, \theta) + \mu_d \phi(\hat{y}) = 0\}$ for $\mu_s > 1$ and $c \in \mathbb{R}^+$ small. The set S_a is a graph over the set of invariant circles of Corollary 3.3 for $c \rightarrow 0$.

Proposition 5.4. *For $0 < \varepsilon \ll 1$ the set S_a perturbs into a slow manifold $S_{a,\varepsilon}$ and on it, there exists a unique, attracting 2π -periodic limit cycle passing through $(x, \theta) = (0, 0) + \mathcal{O}(\varepsilon)$.*

Proof. From Proposition 5.1 and Corollary 3.3 it follows that S_a is filled by circular trajectories. By Fenichel's results, when $0 < \varepsilon \ll 1$ the set S_a perturbs into the graph $\hat{y} = \phi^{-1}(-\xi(x, \theta)/\mu_d) + \varepsilon h_1(x, \theta)$. On this graph the slow problem (11) is a 2π -periodic, non-autonomous ODE for $x(\theta)$, where θ has the meaning of time:

$$(16) \quad x'(\theta) = \varepsilon \phi^{-1} \left(\frac{-\xi(x, \theta)}{\mu_d} \right) + \varepsilon^2 h_1(x, \theta).$$

Fix a global Poincaré section at $\theta = 0$, and define the return map $P(x(0), \varepsilon) = x(2\pi)$. The fixed points of this map for $0 < \varepsilon \ll 1$ are the zeros of the function

$$Q(x(0), \varepsilon) := \frac{P(x(0), \varepsilon) - x(0)}{\varepsilon} = \int_0^{2\pi} \phi^{-1} \left(\frac{-\gamma^2 x(s) - \sin s}{\mu_d} \right) ds + \mathcal{O}(\varepsilon),$$

where the last equality is obtained by integrating (16). For $\varepsilon = 0$, (16) implies $x(\theta) = x(0)$. Both the functions ϕ^{-1} and $\sin s$ are symmetric with respect to the origin. This means that $Q(x(0), 0) = 0$ if and only if $x(0) = 0$. Furthermore $(x(0), 0)$ is regular because

$$(17) \quad \partial_x Q(0, 0) = -\frac{\gamma^2}{\mu_d} \int_0^{2\pi} \frac{1}{\phi'(-\sin s/\mu_d)} ds < 0$$

and $\phi'(\hat{y})$ is always positive in S_a , since $\hat{y} \in]-\delta, \delta[$. Then the Implicit Function Theorem guarantees that for $0 < \varepsilon \ll 1$ there exists $x(0) = m(\varepsilon)$ such that $Q(m(\varepsilon), \varepsilon) = 0$. Hence $x(0) = m(\varepsilon)$ belongs to a stable periodic orbit since from (17) it follows that $|\partial_{x(0)} P(x(0), \varepsilon)| < 1$ for $0 < \varepsilon \ll 1$. ■

Therefore, when $\mu_s > 1$ the family of circles in Σ_s bifurcates into a single attracting limit cycle on the slow manifold $S_{a,\varepsilon}$. This result gives an upper bound of the time T of Proposition 5.3 as a function of ε , since on the slow manifold $S_{a,\varepsilon}$, after a time $t = \mathcal{O}(1/\varepsilon)$, orbits are $\mathcal{O}(1)$ distant to the original family of circles in Σ_s . Furthermore, the regularization of regular stiction solutions does not necessarily remain uniformly close.

It is not possible to make a statement similar to Proposition 5.3 for singular stiction solutions, as they have non-unique forward solutions at the singular level. A further understanding can be obtained by studying the reduced problem (14). This differential algebraic equation, is rewritten as a standard ODE by explicating the algebraic condition with respect to x and by differentiating it with respect to the time t :

$$(18) \quad \begin{aligned} -\mu_d \phi'(\hat{y}) \hat{y}' &= \cos \theta, \\ \theta' &= 1. \end{aligned}$$

Proposition 5.5. *The circles $f^\pm \subset \{\phi'(\hat{y}) = 0\}$ are lines of singularities for the reduced problem (18), and solutions reach them in finite time. On f^\pm , the points $(\hat{y}, \theta) = (-\delta, \pi/2)$ and $(\hat{y}, \theta) = (\delta, 3\pi/2)$ are folded saddles, while $(\hat{y}, \theta) = (\delta, \pi/2)$ and $(\hat{y}, \theta) = (-\delta, 3\pi/2)$ are folded centers. Moreover the intervals $\hat{I}^\pm \subset f^\pm$ defined as*

$$\begin{aligned} \hat{I}^- &:= \{(x, \hat{y}, \theta) \in \mathbb{R}^2 \times \mathbb{T}^1 \mid \xi = \mu_s, \quad \hat{y} = -\delta, \theta \in]\pi/2, 3\pi/2[\}, \\ \hat{I}^+ &:= \{(x, \hat{y}, \theta) \in \mathbb{R}^2 \times \mathbb{T}^1 \mid \xi = -\mu_s, \hat{y} = \delta, \quad \theta \in [0, \pi/2[\cup]3\pi/2, 2\pi[\}, \end{aligned}$$

have non-unique forward solutions.

Proof. The time transformation $\mu_d \phi'(\hat{y}) d\hat{t} = dt$ allows to rewrite system (18) as the desingularized problem

$$(19) \quad \begin{aligned} \dot{\hat{y}} &= -\cos \theta, \\ \dot{\theta} &= \mu_d \phi'(\hat{y}), \end{aligned}$$

in the new time \hat{t} . The difference between system (18) and (19) is that \hat{t} reverses the direction of time within C_r^\pm . Problem (19) has four fixed points in $\mathbb{R}^2 \times \mathbb{T}^1$. The points $(\delta, 3\pi/2)$ and $(-\delta, \pi/2)$ are hyperbolic saddles with eigenvalues $\pm \sqrt{\mu_d |\phi''(\delta)|}$, and eigenvectors respectively $[1, \mp \sqrt{\mu_d |\phi''(\delta)|}]^T$ and $[1, \pm \sqrt{\mu_d |\phi''(\delta)|}]^T$. The remaining points $(\delta, \pi/2)$ and $(-\delta, 3\pi/2)$ are centers with eigenvalues $\pm i \sqrt{\mu_d |\phi''(\delta)|}$, and eigenvectors $[1, \pm i \sqrt{\mu_d |\phi''(\delta)|}]^T$ and $[1, \mp i \sqrt{\mu_d |\phi''(\delta)|}]^T$ respectively. The inversion of the time direction on C_r^\pm gives the dynamics of the reduced problem (18). Thus a saddle in (19) is a folded saddle in (18),

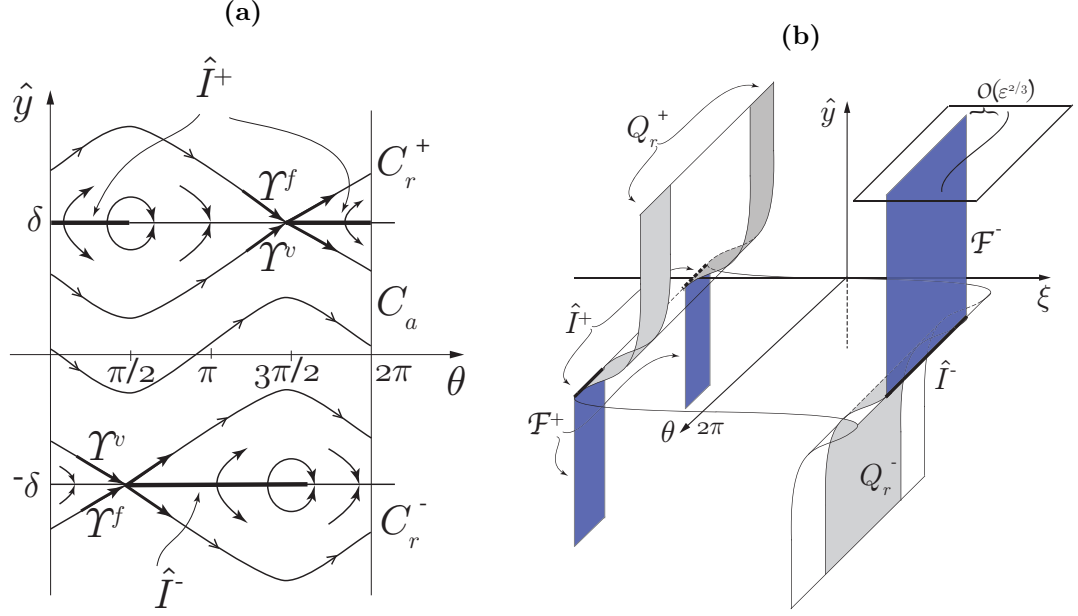


Figure 7: (a): Phase space of the reduced problem (18). (b): repelling invariant manifolds Q_r^\pm in grey, and foliations \mathcal{F}^\pm in blue.

similarly for the centers. Also, f^\pm become lines of singularities with the time inversion, and the segments \hat{I}^\pm have forward trajectories pointing inside both C_a and C_r^\pm , compare with Figure 7(a). Since $\theta' = 1$, orbits reach or leave f^\pm in finite time. ■

Figure 7 illustrates the results of Proposition 5.5. In the (x, y, θ) coordinates, the segments \hat{I}^\pm collapse onto the lines of non-uniqueness I^\pm for $\varepsilon = 0$. The layer problem (13) adds a further forward solution in \hat{I}^\pm , since orbits may also leave a point of these lines by following a fast fiber for $\hat{y} \gtrless 0$.

Each folded saddle has two special solutions: the *singular vrai canard* Υ^v that connects C_a to C_r^\pm , and the *singular faux canard* Υ^f that does the opposite [3, 12]. The vrai canard separates two different types of forward dynamics: on one side of Υ^v orbits *turn*, that means they remain on C_a . On the other side of Υ^v orbits reach $f^\pm \setminus \hat{I}^\pm$ and then *jump*, that is, they move away from C_0 by following a fast fiber. Each singular canard is a periodic orbit that visits both C_a and C_r^\pm , see Figure 7(a). The folded centers have no canard solutions [27] and for this reason they are not interesting for the analysis. Canards are a generic feature of systems with two slow and one fast variable. They appear for instance in the Van der Pol oscillator [19, 46], in a model for global warming [47] and in a model for transonic wind [6].

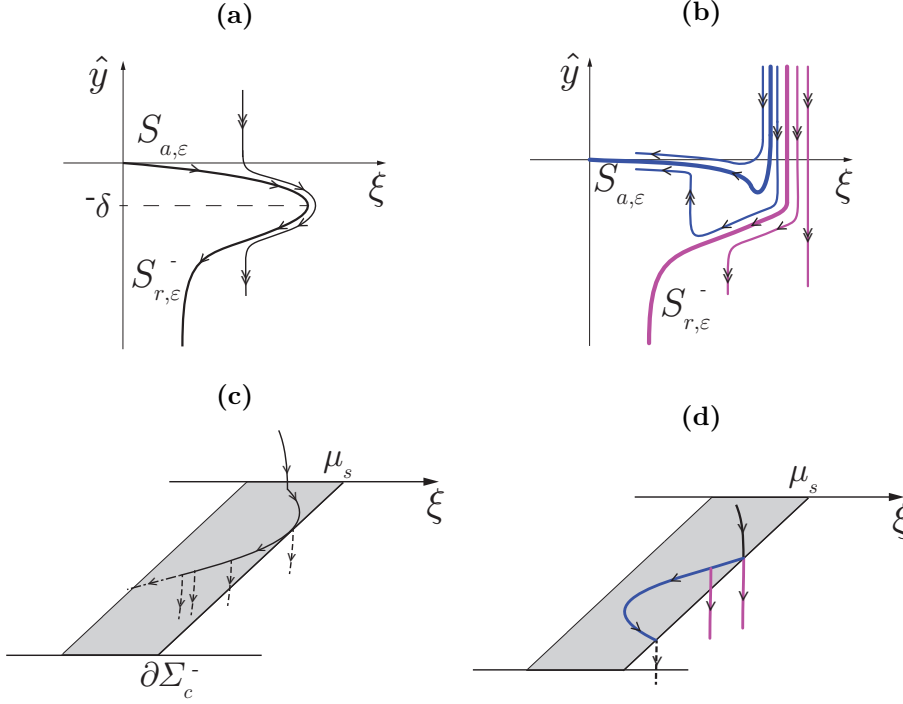


Figure 8: (a): A canard orbit at the intersection of $S_{a,\varepsilon}$ with $S_{r,\varepsilon}^-$. (b): Dynamics around a point of \hat{I}^- , for $0 < \varepsilon \ll 1$. (c) and (d): The same dynamics of Figures 8(a) and 8(b) in the (x, y, θ) -coordinates. The canard-like solutions leaving $\Sigma_{s,\text{stiction}}^-$ resemble Carathéodory solutions of model (4), compare with Figure 4(a).

When $0 < \varepsilon \ll 1$ the singular vrai canard Υ^v perturbs into a maximal canard [43]. This orbit corresponds to the intersection of $S_{a,\varepsilon}$ with $S_{r,\varepsilon}^\pm$. Hence the maximal canard remains $\mathcal{O}(\varepsilon)$ -close to S_r^\pm for a time $t = \mathcal{O}(1)$. Furthermore a family of orbits remains exponentially close to the maximal canard for some time, before being repelled from $S_{r,\varepsilon}^\pm$ [28, p. 200]. An orbit of this family is called a *canard* and Figure 8(a) shows an example of it. Define Q_r^\pm as the subsets of C_r^\pm whose solutions, when flowed backwards in time, intersect the intervals of non-uniqueness \hat{I}^\pm . Q_r^\pm are coloured in grey in Figure 7(b). The lines \hat{I}^\pm are, backwards in time, the base of a foliation of fast fibers \mathcal{F}^\pm , that are coloured in blue in Figure 7(b). The following Proposition describes the role of the repelling manifolds Q_r^\pm for $0 < \varepsilon \ll 1$.

Proposition 5.6. *For $0 < \varepsilon \ll 1$ compact subsets S_r^\pm of Q_r^\pm perturb into the sets $S_{r,\varepsilon}^\pm$ that are $\mathcal{O}(\varepsilon)$ -close to S_r^\pm . The slow problem on $S_{r,\varepsilon}^\pm$ is connected backwards in time to a family of fast trajectories $\mathcal{F}_\varepsilon^\pm$ that is $\mathcal{O}(\varepsilon^{2/3})$ -close to \mathcal{F}^\pm . The orbits on $\mathcal{F}_\varepsilon^\pm$ and $S_{r,\varepsilon}^\pm$ separate the trajectories that, after possibly having been exponentially close to $S_{r,\varepsilon}^\pm$, are attracted to the*

slow manifold $S_{a,\varepsilon}$ to the ones that follow a fast trajectory away from the slow surface.

Proof. By reversing the time orientation on the slow (11) and fast problem (12), the orbits on Q_r^\pm satisfy the assumptions of Proposition 5.3. Hence the distance of \mathcal{F}^\pm to $\mathcal{F}_\varepsilon^\pm$ is $\mathcal{O}(\varepsilon^{2/3})$. Now consider again the true time direction, and take a set of initial conditions that is exponentially close to the fibers $\mathcal{F}_\varepsilon^\pm$. These orbits will follow the repelling slow manifolds $S_{r,\varepsilon}^\pm$ for a time $t = \mathcal{O}(1)$ [43]. The manifolds $S_{r,\varepsilon}^\pm$ act as separators of two different futures: on one side the orbits will get attracted to the slow attracting manifold $S_{a,\varepsilon}$, while on the other side they will jump away by following an escaping fast fiber, compare with Figure 8(b). ■

It follows that around \hat{I}^\pm and \mathcal{F}^\pm there is a high sensitivity to the initial conditions. Even though the (x, θ) -dynamics on C_a coincides with the one on C_r^\pm , trajectories close to these two manifolds may have different futures. Orbits belonging to $S_{a,\varepsilon}$ will exit $S_{a,\varepsilon}$ in a predictable point. On the other hand, the orbits that follow $S_{r,\varepsilon}^\pm$ are very sensitive, and may escape from it at any time. These two types of trajectories are coloured respectively in blue and magenta in Figures 8(b) and 8(d). The orbits that follow $S_{r,\varepsilon}^\pm$ for some time are canard-like in the forward behaviour. However in backward time they are connected to a family of fast fibers instead than to $S_{a,\varepsilon}$ and for this reason they are not typical canards like Υ^v .

In the original coordinates (x, y, θ) , the canard trajectories of the folded saddles and the canard-like solutions of the lines \hat{I}^\pm leave the slow manifold in a point inside $\Sigma_{s,stick}^\pm$, as in Figures 8(c) and 8(d). In the piecewise smooth system these orbits satisfy the Carathéodory condition (7) but they are not stiction solutions. It follows that some of the Carathéodory solutions of (4) appear upon regularization of the stiction model: these are the trajectories of Z_s that intersect I^\pm backwards in time. All the other Carathéodory solutions of model (4) do not have a corresponding solution in the regularized model. The interpretation of the solutions with canard is that the slip onset is delayed with respect to the time when the external forces have equalled the maximum static friction force. Figure 11(c) in subsection 6.1, will show a numerical solution having this delay.

6. Slip-stick periodic orbits. This section considers a family of periodic orbits of model (4) that interacts with the lines of non-uniqueness I^\pm . Then subsection 6.1 discusses how the family perturbs in the regularized system (10) for $0 < \varepsilon \ll 1$, by combining numerics and analysis.

Model (4) has several kinds of periodic motion: pure slip [8, 41], pure stick [22], non-symmetric slip-stick [2, 17, 33, 34, 37], symmetric slip-stick [22, 34]. This section focuses on the latter, as slip-stick orbits are likely to be affected by the non-uniqueness at I^\pm . Figure 9 shows an example of such a trajectory. The symmetric slip-stick trajectories can be found by solving a system of algebraic equations, because system (4), in its non-autonomous form, is piecewise-linear in each region. Furthermore, it is sufficient to study only half the period, as ensured by the following two Lemmas 6.1 and 6.2.

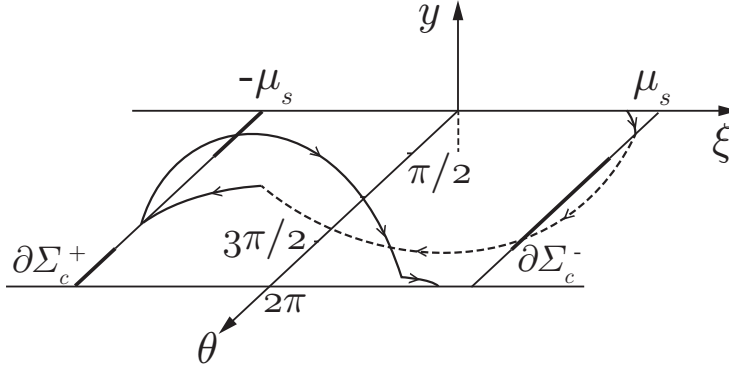


Figure 9: A symmetric, slip-stick, periodic orbit with $\theta \in \mathbb{T}^1$. The dashed line represents trajectories in Z^- . The interest is to study how such orbit interacts with the intervals of non-uniqueness I^\pm (in bold) under variation of a parameter.

Lemma 6.1. *System (4) has a symmetry*

$$(20) \quad S(x, y, \theta) = (-x, -y, \theta + \pi).$$

Proof. The map (20) is a diffeomorphism $\mathbb{R}^2 \times \mathbb{T}^1 \rightarrow \mathbb{R}^2 \times \mathbb{T}^1$ that satisfies the condition for a symmetry $Z(S(z)) = DS(z)Z(z)$, where $DS(z)$ is the Jacobian of $S(z)$ and $z = (x, y, \theta)$ [31, p. 211]. ■

Lemma 6.2. *Let $\varphi_t(z)$ be the regular stiction orbit of system (4) at time t , with initial condition $z = (x, y, \theta)$. If $\varphi_\pi(z) = (-x, -y, \theta + \pi)$ then the orbit is symmetric and periodic with period $T = 2\pi$.*

Proof. Applying the symmetry map (20) to the point $\varphi_\pi(z)$, gives

$$S(-x, -y, \theta + \pi) = (x, y, \theta + 2\pi).$$

Since $Z(x, y, \theta + 2\pi) \equiv Z(x, y, \theta)$ for any $\theta \in \mathbb{T}^1$, the flow $\varphi_t(z)$ is symmetric and periodic, with symmetry (20) and period $T = 2\pi$. ■

The results of Lemma 6.2 have been used in [41] even though the symmetry was not made explicit. Define $\varphi_t^{\text{slip}}(z_0)$ (resp. $\varphi_t^{\text{stick}}(z_1)$) the slip (stick) solution of $Z^-(z)$ ($Z_s(z)$) with initial conditions in z_0 (z_1). The following Lemma states when these two solutions, pieced together, belong to a symmetric slip-stick periodic orbit.

Lemma 6.3. *Necessary conditions for the slip and stick solutions $\varphi_t^{\text{slip}}(z_0)$ and $\varphi_t^{\text{stick}}(z_1)$*

Table 1: Parameters values used in the simulations.

μ_s	μ_d	ε	δ
1.1	0.4	10^{-3}	0.6

to form the lower half of a symmetric, slip-stick, periodic orbit are

$$(21a) \quad \varphi_{\pi-\theta^*}^{slip}(z_0) = \varphi_0^{stick}(z_1),$$

$$(21b) \quad \varphi_{\theta^*}^{stick}(z_1) = S(z_0).$$

where $0 < \theta^* < \pi$ is the duration of one stick phase and $z_0 \in \partial\Sigma_c^-$, $z_1 \in \Sigma_s$.

Condition (21a) guarantees the continuity between the stick and slip phase, while (21b) guarantees the symmetry. The upper half-period of the orbit follows by applying the symmetry map (20) to φ_t^{slip} and φ_t^{stick} .

Corollary 6.4. *Conditions (21) are equivalent to*

$$(22a) \quad x^{slip}(\pi - \theta^*) = -x_0,$$

$$(22b) \quad y^{slip}(\pi - \theta^*) = 0,$$

$$(22c) \quad \pi - \theta^* + \theta_0 = \theta_1.$$

Where $z_0 = (x_0, y_0, \theta_0) \in \Sigma_c^-$, $z_1 = (x_1, y_1, \theta_1) \in \Sigma_s$ and $\varphi_t^{slip}(z_0) = (x(t), y(t), \theta(t))^{slip}$.

Proof. The stick solution of (4) with initial condition $z_1 = (x_1, 0, \theta_1)$ is $(x, y, \theta)^{stick}(t) = (x_1, 0, t + \theta_1)$. Condition (21a) then implies that $x^{slip}(\pi - \theta^*) = x_1$ and $y^{slip}(\pi - \theta^*) = 0$, while $\theta^{slip}(\pi - \theta^*) = \pi - \theta^* + \theta_0 = \theta_1$. Condition (21b) adds furthermore that $x_1 = -x_0$. ■

The stick-slip solutions of (4) are now investigated numerically. The system of conditions (22) has five unknown parameters: $\gamma, \theta_0, \theta^*, \mu_s$ and μ_d . It is reasonable to fix μ_s and μ_d as these are related to the material used, and then find a family of solutions of (22) by varying the frequency ratio $\gamma = \Omega/\omega$. The values used in the computations are listed in Table 1. Notice that conditions (22) are necessary but not sufficient: further admissibility conditions may be needed. These are conditions that control that each piece of solution does not exit its region of definition, for example: the stick solution should not cross $\partial\Sigma_c^-$ before $t = \theta^*$, and should not cross $\partial\Sigma_c^+$ for any $t \in [0, \theta^*]$. A numerical computation shows that system (22) has two branches of solutions $\Pi_0^{l,r}$, as shown in Figure 10: one for $\gamma < 1$ and one for $\gamma > 1$. The branches are disconnected around the resonance for $\gamma = 1$, where chaotic behaviour may appear [2, 8, 33]. The branch Π_0^l for $\gamma < 1$ is bounded by pure slip orbits when $\theta^* \rightarrow 0$, and by the visible tangency on Σ_s when $\theta_0 \rightarrow \pi/2$. The latter is marked with a circle in Figure 10(a). The branch Π_0^r for $\gamma > 1$ is delimited by pure slip orbits when $\gamma \rightarrow 1$ since again $\theta^* \rightarrow 0$, while when $\gamma \gg 1$, that is the rigid body limit, the

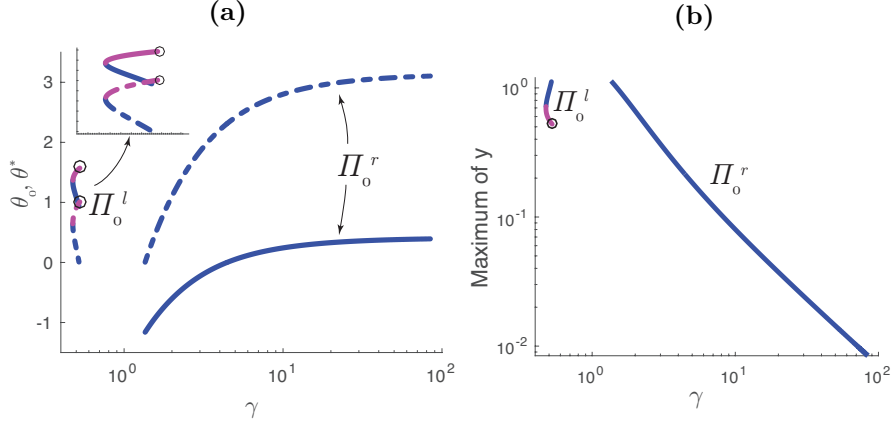


Figure 10: (a): Two families of slip-stick orbits $\Pi_0^{l,r}$ of (4) for $\mu_s = 1.1$, $\mu_d = 0.4$. The solid line is θ_0 while the dashed line is θ^* . The blue denotes a stable periodic orbit, while the magenta a saddle periodic orbit. (b): Maximum amplitude of the orbits.

family is bounded by $\theta^* \rightarrow \pi$. Here periodic orbits have a very short slip phase and an almost π -long stick phase.

A slip-stick orbit of model (4) has three Floquet multipliers. Of these, one is trivially unitary, the second one is always zero and the last indicates the stability of the periodic orbit. The zero multiplier is due to the interaction of the periodic orbit with the sticking manifold Σ_s : solutions lying on this surface are backwards non-unique. Figure 10 denotes in blue the attracting periodic solutions and in magenta the repelling ones. In particular the family Π_0^l becomes unstable sufficiently close to the visible tangency at $\theta_0 = \pi/2$, which is marked with a circle in Figure 10. This is because the visible tangency acts as a separatrix of two very different behaviours: on one side orbits jump, while on the other side they turn, recall Figure 7(a).

6.1. Slip-stick periodic orbits in the regularized system. This section finds slip-stick periodic solutions of the regularized model (10) with a numerical continuation in AUTO [10]. The solutions are then compared with the ones of the discontinuous system (4). The regularization function used is a polynomial

$$\phi(y) = y(ay^6 + by^4 + cy^2 + d),$$

within $y \in [-1, 1]$, where the coefficients a, b, c, d are determined by the conditions (9) for the parameters listed in Table 1. Hence $\phi(y)$ is C^1 for $y \in \mathbb{R}$. Figure 11(a) shows the family of slip-stick periodic orbits Π_ε of system Figure 11(a). This can be seen, loosely, as the union of three branches

$$\Pi_\varepsilon = \Pi_\varepsilon^l \cup \Pi_\varepsilon^c \cup \Pi_\varepsilon^r,$$

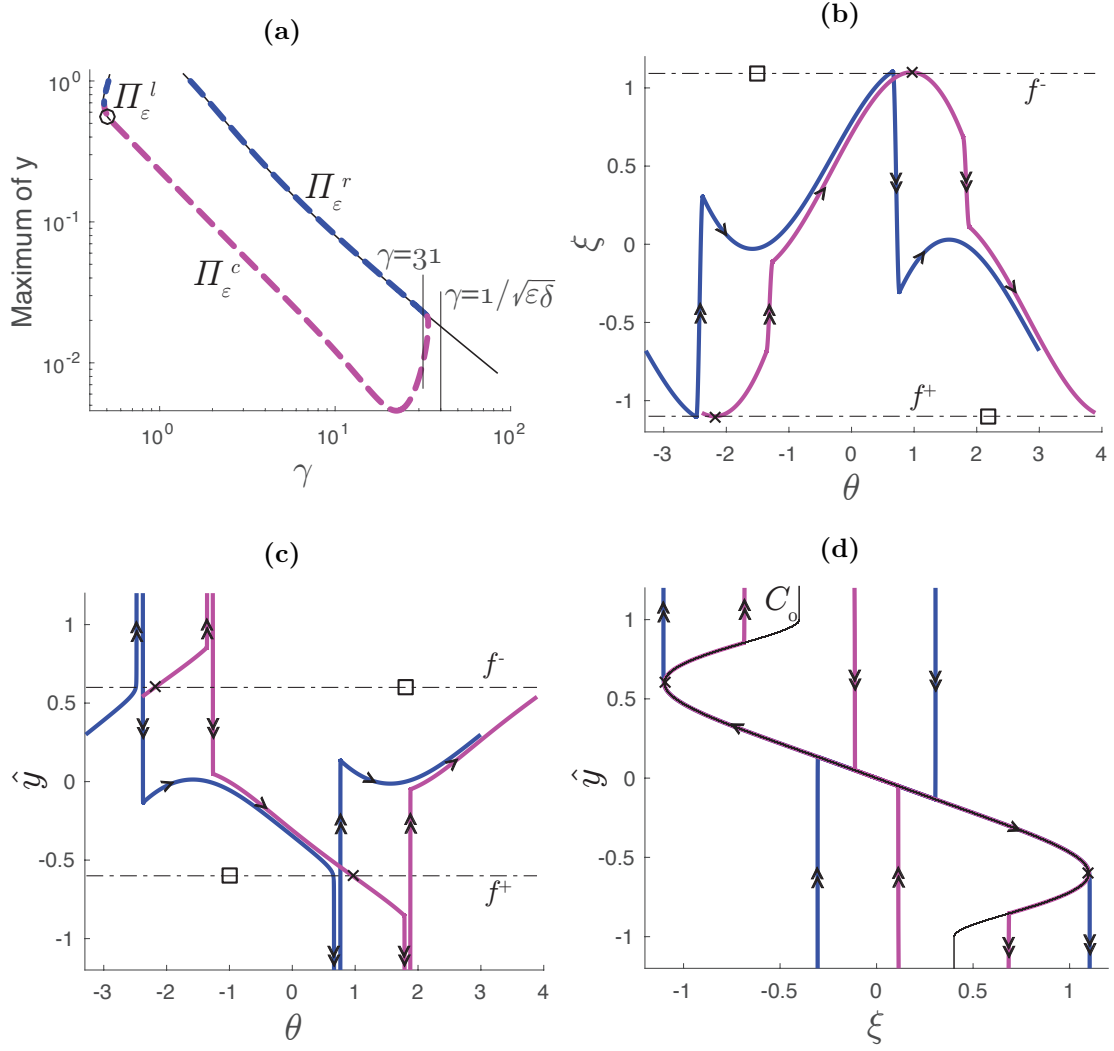


Figure 11: Numerical simulation in AUTO. (a): In dashed the family Π_ε . The repelling branch Π_ε^c connects the two regular branches $\Pi_\varepsilon^{l,r}$. Solid line: families $\Pi_0^{l,r}$. The colours denote the stability of the orbits, as in Figure 10. (b): Two periodic orbits co-existing for $\gamma = 31$: a regular slip-stick in blue and a slip-stick with canard segments in magenta. The x marks the folded saddle while the \square denotes the folded node. (c) and (d): Projections of (b) in the (θ, \hat{y}) and (ξ, \hat{y}) -plane.

where $\Pi_\varepsilon^{l,r}$ are $\mathcal{O}(\varepsilon^{2/3})$ -close to the regular branches $\Pi_0^{l,r}$ [44]. The branch Π_ε^c connects Π_ε^l to Π_ε^r at the rigid body limit, that is $\gamma \gg 1$, and it consists of slip-stick periodic orbits each having two canard segments. Figures 11(b) to 11(d) show for $\gamma = 31$ two

co-existing periodic orbits: the magenta one belongs to Π_ε^c and the blue one belongs to Π_ε^r . In particular Figure 11(c) shows the delay in the slip onset, when the orbit follows the canard, since the slip happens after a time $t = \mathcal{O}(1)$ with respect to when the orbit has intersected the fold lines f^\pm .

The existence of the branch Π_ε^c is supported by the next Proposition 6.5. For this, let Σ_{out} be a cross-section orthogonal to the y -axis, so that the fast fibers with base on the singular vrai canard on C_r^- , intersect it on the line $L_{\text{out},0}$. Furthermore, define Σ_{in} the cross-section orthogonal to the ξ -axis so that it intersects C_a on the line $L_{\text{in},0}$, see Figure 12(a).

Proposition 6.5. *Suppose that for $\varepsilon = 0$ there exists a smooth return mechanism $R : \Sigma_{\text{out}} \rightarrow \Sigma_{\text{in}}$ that maps $L_{\text{out},0} \subset \Sigma_{\text{out}}$ onto $L_{\text{in},0} \subset \Sigma_{\text{in}}$. Suppose furthermore that $L_{\text{in},0} = R(L_{\text{out},0})$ is transversal to the singular vrai canard Υ^v . Then for $0 < \varepsilon \ll 1$ there exists a unique, periodic orbit $\varphi_t^\varepsilon(z)$ that has a canard segment, and that tends to the singular canard for $\varepsilon \rightarrow 0$. Furthermore this orbit has a saddle stability with Floquet multipliers: $\{1, \mathcal{O}(e^{-c_1/\varepsilon}), \mathcal{O}(e^{c_2/\varepsilon})\}$, with $c_{1,2} \in \mathbb{R}^+$.*

Proof. First notice that for $0 < \varepsilon \ll 1$ the singular vrai canard Υ^v on C_r^- perturbs into a maximal canard that is $\mathcal{O}(\varepsilon^{2/3})$ -close to it. This maximal canard is the base of a foliation of fibers that intersect Σ_{out} on a line $L_{\text{out},\varepsilon}$ that is $\mathcal{O}(\varepsilon^{2/3})$ -close to $L_{\text{out},0}$. The return map $R(z)$ is smooth, so that $R(L_{\text{out},\varepsilon})$ intersects Σ_{in} in a line $L_{\text{in},\varepsilon}$ that is $\mathcal{O}(\varepsilon^{2/3})$ -close to $L_{\text{in},0}$. The line $L_{\text{in},\varepsilon}$ is transversal to the maximal canard for ε sufficiently small, since $L_{\text{in},0}$ was transversal to Υ^v , and the perturbation is $\mathcal{O}(\varepsilon^{2/3})$.

Now consider the backward flow of $L_{\text{out},\varepsilon}$. This contracts to the maximal canard with an order $\mathcal{O}(e^{-c/\varepsilon})$. Hence it intersects $L_{\text{in},\varepsilon}$ in an exponentially small set that is centered around the maximal canard. This means that the reduced Poincaré map $P : L_{\text{in},\varepsilon} \rightarrow L_{\text{in},\varepsilon}$ is well defined and contractive in backwards time. Hence it has a unique fixed point. Such fixed point corresponds to a periodic orbit with canard. It follows that the periodic orbit has an exponential contraction to the attracting slow manifold, and an exponential repulsion forward in time around the maximal canard. This determines the Floquet multipliers and consequently, the saddle stability. ■

Figure 12(b) shows numerically that the discontinuous model (4) satisfies the assumptions of Proposition 6.5. This supports the existence of the branch Π_ε^c in the regularized model for ε sufficiently small. Because of the symmetry, the branch Π_ε^c has two canards segments for each period. A *canard explosion* may appear when a family of periodic orbits interacts with a canard. The explosion is defined as the transition from a small oscillation to a relaxation oscillation for an exponentially small variation in the parameter [26]. However system (10) has no canard explosion: Figure 11(a) shows that the maximum amplitude of the oscillations does not increase with the continuation from Π_ε^l to Π_ε^c . The effect of the canard is instead in the explosion of one of the Floquet multipliers as previously stated in Proposition 6.5, and observed numerically in AUTO. The saddle stability of the family Π_ε^c implies that the periodic orbits of Π_ε^c are always repelling, even with a time inversion. Hence these periodic orbits are not visible in standard simulations. It could be interesting

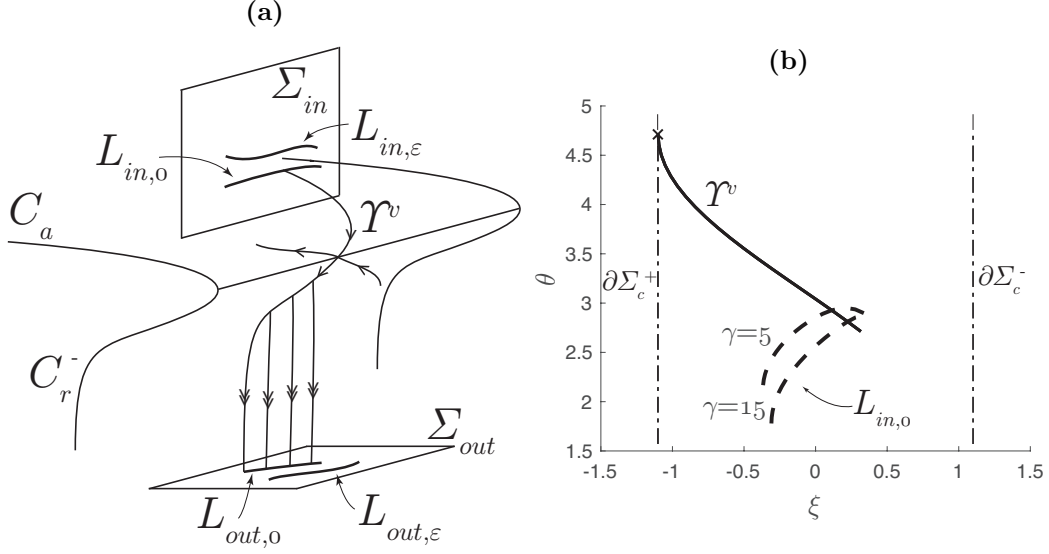


Figure 12: (a): Construction of the cross-sections $\Sigma_{in,out}$. (b): Numerical simulation showing that $R(L_{out,0})$ (dashed line) is transversal to Υ^v (solid line) for $\varepsilon = 0$ and $\gamma = \{5, 15\}$. The visible tangency is marked with x . The dashed-dotted lines are $\partial\Sigma_c^\pm$.

to make an experiment, with very high precision in the initial conditions, where the effects of the canard are measurable. If canard solutions appear, then this would support the validity of the stiction model and of its regularization.

Proposition 6.6. *The branch Π_ε^c is bounded above by $\gamma = 1/\sqrt{\varepsilon\delta}$ for $0 < \varepsilon \ll 1$.*

Proof. Differentiate $\xi(x, \theta) = \gamma^2 x + \sin(\theta)$ with respect to time, and rewrite the slow problem (11) in the (ξ, \hat{y}, θ) variables

$$\begin{aligned}\xi' &= \gamma^2 \varepsilon \hat{y} + \cos \theta, \\ \varepsilon \hat{y}' &= -\xi - \mu_d \phi(\hat{y}), \\ \theta' &= 1.\end{aligned}$$

If $\gamma^2 = \mathcal{O}(1/\varepsilon)$, it makes sense to introduce the rescaling $\Gamma := \gamma^2 \varepsilon$, so that the slow problem becomes

$$\begin{aligned}\xi' &= \Gamma \hat{y} + \cos \theta, \\ \varepsilon \hat{y}' &= -\xi - \mu_d \phi(\hat{y}), \\ \theta' &= 1.\end{aligned}$$

This system has again a multiple time-scale with critical manifold (15). Its reduced problem

in the time \hat{t} is

$$(23) \quad \begin{aligned} \dot{\hat{y}} &= -\Gamma \hat{y} - \cos \theta, \\ \dot{\theta} &= \mu_d \phi'(\hat{y}). \end{aligned}$$

Notice that (23) differs from the desingularized problem (19) only for the term $\Gamma \hat{y}$ in the \hat{y} dynamics. The fixed points of (23) exist if $|\Gamma \delta| \leq 1$ and they have coordinates $\hat{y} = \pm \delta$, $\cos \theta = \mp \Gamma \delta$. The comparison of system (23) with the desingularized problem (19) shows that the fixed points have shifted along the θ -direction. In particular the saddles have moved backwards while the centers have moved forward. Furthermore the centers have become stable foci. For increasing values of Γ the stable foci turn into stable nodes. When $|\Gamma \delta| = 1$ pairs of saddles and nodes collide and disappear through a saddle-node bifurcation of type I [28, Lemma 8.5.7]. Beyond this value canard solutions cease to exist. Such a condition is equivalent to $\gamma = 1/\sqrt{\varepsilon \delta}$. ■

The bound $\gamma = 1/\sqrt{\varepsilon \delta}$, that is highlighted in Figure 11(b), is larger than the value of γ for which the family Π_ε^c folds. In particular, at the turning point, the folded foci have not turned into folded nodes yet. Thus the collision of the folded saddles with the folded foci is not a direct cause of the saddle-node bifurcation of Π_ε^c , but gives only an upper bound for the existence of the family. When the folded nodes appear, there might exist further periodic orbits that exit the slow regime through the canard associated to the stable nodes. Furthermore, the orbits of Π_ε^c interact with the folded saddle only, but they do not interact with the other points of \hat{I}^\pm . The regularized problem (10) may have other families of periodic orbits that interact with \hat{I}^\pm . For example, a family of pure slip periodic orbits, that reaches \hat{I}^\pm from a fast fiber and then jumps off through a canard-like solution. However, this family would also turn unstable when passing sufficiently close to the canards, because of the high sensitivity to the initial conditions around \mathcal{F}^\pm . In particular an explosion in the Floquet multipliers is again expected, because of Proposition 6.5.

7. Conclusions. Stiction is a widely used formulation of the friction force, because of its simplicity. However this friction law has issues of non-uniqueness at the slip onset, that in this manuscript are highlighted in a friction oscillator model. This model is a discontinuous, non-Filippov system, with subregions having a non-unique forward flow. The forward non-uniqueness is problematic in numerical simulations: here a choice is required and hence valid solutions may be discarded. A regularization of the model resolves the non-uniqueness by finding a repelling slow manifold that separates forward sticking to forward slipping solutions. Around the slow manifold there is a high sensitivity to the initial conditions. Some trajectories remain close to this slow manifold for some time before being repelled. These trajectories, that mathematically are known as canards, have the physical interpretation of delaying the slip onset when the external forces have equalled the maximum static friction force at stick. This result could potentially be verified experimentally, thus furthering the understanding of friction-related phenomena. Indeed the appearance of the canard solutions is a feature of stiction friction rather than of the specific friction

oscillator model. For example the addition of a damping term on the friction oscillator, or the problem of a mass on an oscillating belt would give rise to similar canard solutions. The canard solutions of the regularized systems can be interpreted, in the discontinuous model, as Carathéodory trajectories that allow the slip onset in points inside the sticking region. These Carathéodory orbits are identified by being backwards transverse to the lines of non-uniqueness.

The manuscript shows also that the regularized system has a family of periodic orbits Π_ε interacting with the folded saddles. The orbits with canard $\Pi_\varepsilon^c \subset \Pi_\varepsilon$ have a saddle stability, with Floquet multipliers $\mathcal{O}(e^{\pm c\varepsilon^{-1}})$. Furthermore, the family Π_ε^c connects, at the rigid body limit, the two families of slip-stick periodic orbits $\Pi_0^{l,r}$ of the discontinuous problem. Further periodic orbits may interact with the canard segments.

Acknowledgments. The first author thanks Thibault Putelat and Alessandro Colombo for the useful discussions. We acknowledge the Idella Foundation for supporting the research. This research was partially done whilst the first author was a visiting researcher at the Centre de Recerca Matemàtica in the Intensive Research Program on Advances in Nonsmooth Dynamics.

References.

REFERENCES

- [1] A. AKAY, *Acoustics of friction*, J. Acoust. Soc. Am., 111 (2002), pp. 1525–1548.
- [2] U. ANDREAS AND P. CASINI, *Dynamics of friction oscillators excited by a moving base and/or driving force*, J. Sound Vibration, 245 (2001), pp. 685–699.
- [3] E. BENOÎT, J. F. CALLOT, F. DIENER, AND M. DIENER, *Chasse au canard*, Collectanea Mathematica, 32 (1981), pp. 37–119.
- [4] P. A. BLIMAN AND M. SORINE, *Easy-to-use realistic dry friction models for automatic control*, in Proceedings of the 3rd European Control Conference, 1995, pp. 3778–3794.
- [5] C. CANTONI, R. CESARINI, G. MASTINU, G. ROCCA, AND R. SICIGLIANO, *Brake comfort - a review*, Vehicle Sys Dyn, 47 (2009), pp. 901–947.
- [6] P. CARTER, E. KNOBLOCH, AND M. WECHSELBERGER, *Transonic canards and stellar wind*, Nonlinearity, 30 (2017), p. 1006.
- [7] J. CORTES, *Discontinuous dynamical systems*, IEEE Control Systems, 28 (2008), pp. 36–73.
- [8] G. CSERNÁK AND G. STÉPÁN, *On the periodic response of a harmonically excited dry friction oscillator*, J. Sound Vibration, 295 (2006), pp. 649–658.
- [9] G. CSERNÁK, G. STÉPÁN, AND S. W. SHAW, *Sub-harmonic resonant solutions of a harmonically excited dry friction oscillator*, Nonlinear Dyn, 50 (2007), pp. 93–109.
- [10] E. J. DEODEL, *Lecture notes on numerical analysis of nonlinear equations*, in Numerical Continuation Methods for Dynamical Systems, B. Krauskopf, H. M. Osinga, and J. Galán-Vioque, eds., Springer Netherlands, 2016, pp. 1–49.
- [11] M. DI BERNARDO, C. BUDD, A. R. CHAMPNEYS, AND P. KOWALCZYK, *Piecewise-smooth Dynamical Systems*, Springer-Verlag London, 2008.
- [12] F. DUMORTIER AND R. ROUSSARIE, *Canard cycles and center manifolds*, Mem. Amer. Math. Soc, 121 (1996).
- [13] B. FEENY, A. GURAN, N. HINRICHS, AND K. POPP, *A historical review on dry friction and stick-slip phenomena*, Appl. Mech. Rev., 51 (1998), pp. 321–341.

- [14] N. FENICHEL, *Asymptotic stability with rate conditions for dynamical systems*, Bull. Amer. Math. Soc., 80 (1974), pp. 346–349.
- [15] ———, *Geometric singular perturbation theory for ordinary differential equations*, J. Differential Equations, 31 (1979), pp. 53–98.
- [16] A. F. FILIPPOV, *Differential Equations with Discontinuous Righthand Sides*, Springer Netherlands, 1988.
- [17] U. GALVANETTO AND S. R. BISHOP, *Dynamics of a simple damped oscillator undergoing stick-slip vibrations*, Meccanica, 34 (1999), pp. 337–347.
- [18] M. GUARDIA, S. J. HOGAN, AND T. M. SEARA, *An analytical approach to codimension-2 sliding bifurcations in the dry-friction oscillator*, SIAM J. Appl. Dyn. Syst., 9 (2010), pp. 769–798.
- [19] J. GUCKENHEIMER, K. HOFFMAN, AND W. WECKESSER, *Bifurcations of relaxation oscillations near folded saddles*, Int. J. Bifurcation Chaos, 15 (2005), pp. 3411–3421.
- [20] M. A. HECKL AND I. D. ABRAHAMS, *Curve squeal of train wheels, part 1: Mathematical model for its generation*, J. Sound Vibration, 229 (2000), pp. 669–693.
- [21] N. HINRICHS, M. OESTREICH, AND K. POPP, *Experimental and numerical investigation of a friction oscillator*, American Society of Mechanical Engineers, Design Engineering Division (publication) De, 90 (1996), pp. 57–62.
- [22] ———, *On the modelling of friction oscillators*, J. Sound Vibration, 216 (1998), pp. 435–459.
- [23] C. K. R. T. JONES, *Geometric singular perturbation theory*, in Dynamical Systems, R. Johnson, ed., no. 1609 in Lecture Notes in Mathematics, Springer Berlin Heidelberg, 1995, pp. 44–118.
- [24] P. KOWALCZYK AND P. T. PIROINEN, *Two-parameter sliding bifurcations of periodic solutions in a dry-friction oscillator*, Phys. D, 237 (2008), pp. 1053–1073.
- [25] K. U. KRISTIANSEN AND S. J. HOGAN, *On the use of blow up to study regularizations of singularities of piecewise smooth dynamical systems in \mathbb{R}^3* , SIAM J. Appl. Dyn. Syst., 14 (2015), pp. 382–422.
- [26] M. KRUPA AND P. SZMOLYAN, *Relaxation oscillation and canard explosion*, J. Differential Equations, 174 (2001), pp. 312–368.
- [27] M. KRUPA AND M. WECHSELBERGER, *Local analysis near a folded saddle-node singularity*, J. Differential Equations, 248 (2010), pp. 2841–2888.
- [28] C. KUEHN, *Multiple Time Scale Dynamics*, Springer International Publishing, 2015.
- [29] G. LICSKÓ AND G. CSERNÁK, *On the chaotic behaviour of a simple dry-friction oscillator*, Math. Comput. Simulation, 95 (2014), pp. 55–62.
- [30] J. LLIBRE, P. R. DA SILVA, AND M. A. TEIXEIRA, *Sliding vector fields via slow-fast systems*, Bull. Belg. Math. Soc. Simon Stevin, 15 (2008), pp. 851–869.
- [31] J. D. MEISS, *Differential dynamical systems*, SIAM in Mathematical Modeling and Computation, 2007.
- [32] M. NAKATANI, *Conceptual and physical clarification of rate and state friction: Frictional sliding as a thermally activated rheology*, J. Geophys. Res. Solid Earth, 106 (2001), pp. 13347–13380.
- [33] M. OESTREICH, N. HINRICHS, AND K. POPP, *Bifurcation and stability analysis for a non-smooth friction oscillator*, Arch. Appl. Mech., 66 (1996), pp. 301–314.
- [34] H. OLSSON AND K. J. ÅSTRÖM, *Friction generated limit cycles*, IEEE Trans. Control Syst. Technol., 9 (2002), pp. 629–636.
- [35] H. OLSSON, K. J. ÅSTRÖM, C. CANUDAS DE WIT, M. GÄFVERT, AND P. LISCHINSKY, *Friction models and friction compensation*, European J. Control, 4 (1998), pp. 176–195.
- [36] E. PENNESTRÌ, V. ROSSI, P. SALVINI, AND P. P. VALENTINI, *Review and comparison of dry friction force models*, Nonlinear Dyn, 83 (2016), pp. 1785–1801.
- [37] K. POPP AND P. STELTER, *Stick-slip vibrations and chaos*, Philos. Trans. Roy. Soc. London Ser. A, 332 (1990), pp. 89–105.
- [38] T. K. PRATT AND R. WILLIAMS, *Non-linear analysis of stick/slip motion*, J. Sound Vibration, 74 (1981), pp. 531–542.
- [39] T. PUTELAT, J. H. P. DAWES, AND J. R. WILLIS, *Regimes of frictional sliding of a spring-block*

- system, J. Mech. Phys. Solids, 58 (2010), pp. 27–53.
- [40] E. RABINOWICZ, *The nature of the static and kinetic coefficients of friction*, J. Appl. Phys., 22 (1951), pp. 1373–1379.
 - [41] S. W. SHAW, *On the dynamic response of a system with dry friction*, J. Sound Vibration, 108 (1986), pp. 305–325.
 - [42] J. SOTOMAYOR AND M. A. TEIXEIRA, *Regularization of discontinuous vector fields*, in International Conference on Differential Equations (Lisboa), World Scientific, 1996, pp. 207–223.
 - [43] P. SZMOLYAN AND M. WECHSELBERGER, *Canards in \mathbb{R}^3* , J. Differential Equations, 177 (2001), pp. 419–453.
 - [44] ———, *Relaxation oscillations in \mathbb{R}^3* , J. Differential Equations, 200 (2004), pp. 69–104.
 - [45] M. A. TEIXEIRA, *Generic bifurcation of sliding vector-fields*, J. Math. Anal. Appl., 176 (1993), pp. 436–457.
 - [46] T. VO AND M. WECHSELBERGER, *Canards of folded saddle-node type I*, SIAM J. Math. Anal., 47 (2015), pp. 3235–3283.
 - [47] S. WIECZOREK, P. ASHWIN, C. M. LUKE, AND P. M. COX, *Excitability in ramped systems: the compost-bomb instability*, Proc. R. Soc. A, 467 (2011), pp. 1243–1269.
 - [48] J. WOJEWODA, A. STEFAŃSKI, M. WIERCIGROCH, AND T. KAPITANIAK, *Hysteretic effects of dry friction: modelling and experimental studies*, Phil. Trans. R. Soc. A, 366 (2008), pp. 747–765.
 - [49] J. WOODHOUSE, T. PUTLAT, AND A. MCKAY, *Are there reliable constitutive laws for dynamic friction?*, Phil. Trans. R. Soc. A, 373 (2015), p. 20140401.